BER the international journal of bridge engineering management and research

Static and Seismic Analysis of a Cable-Stayed Bridge Equipped with Novel Hybrid Cables

Sourabh Vern[1,*]; Fabrizio Paolacci[1]; Gianluca Quinci[1]; Roberto Nascimbene[2] and Jan Ferino[3]

Submitted: 15 December 2025 **Accepted:** 18 March 2026 **Publication date:** 10 April 2026

DOI: 10.70465/ber.v3i2.73

Abstract: This study investigates the structural performance of a cable-stayed bridge equipped with the hybrid stay cables (HSCs) under both static and seismic conditions within the EU FIRST-WIRE (FIber-Reinforced STeel WIRE) project. Full-scale experimental tests were conducted to assess its performance, followed by finite element modeling of a pedestrian bridge using three cable types: full steel (steel stay cable [SSC]), hybrid (HSC), and full carbon fiber–reinforced polymer (CFRP). Static and dynamic responses were compared across configurations, focusing on force distribution, displacement, stress patterns, and modal frequencies. HSC cables achieved tensile strengths up to 1400 MPa and demonstrated uniform force distribution across varying lengths. Under seismic loads, HSC and CFRP systems produced frequency shifts of 5%–7% and reduced displacements by up to 20% at critical sections. Corrosion simulations for SSC showed over 25% increases in deck moment under 40% material loss, while HSC remained structurally stable. These results highlight the potential of hybrid cables as a balanced solution that combines mechanical efficiency, seismic resilience, and durability, particularly in retrofit applications.

Author keywords: Strengthening; bridge engineering; cable-stayed bridges; earthquake engineering applications

List of Abbreviations

CFRP	Carbon fiber–reinforced polymers
CS	Construction stage
FIRST-WIRE	FIber-Reinforced STeel WIRE
F-CSA	Forward construction stage analysis
FLC	Fully locked coil
HSC	Hybrid stay cable
OSS	Open spiral strands
PGA	Peak ground acceleration
SSC	Steel stay cable
TF	Transmissibility function
ULM	Unknown load method
ε_{hybrid}, ε_{core}, and ε_{tube}	Strain in hybrid, core, and tube section
F_{hybrid}, F_{core}, and F_{tube}	Force in hybrid, core, and tube section
A_{hybrid}, A_{core}, and A_{tube}	Area of hybrid, core, and tube section

*Corresponding Author: Sourabh Vern.
Email: sourabh.vern@gmail.com
[1]Department of Civil, Computer Science and Aeronautical Technologies Engineering, Roma Tre University, Via Vito Volterra 62, Rome, 00146, Italy
[2]University School for Advanced Studies (IUSS), Piazza Della Vittoria 15, Pavia, 27100, Italy
[3]Astarte Strategies S.r.l, Via San Saturnino, 7, Cagliari, 09124, Italy

Discussion period open till six months from the publication date. Please submit separate discussion for each individual paper. This paper is a part of the Vol. 3 of the International Journal of Bridge Engineering, Management and Research (© BER), ISSN 3065-0569.

Introduction

Background and motivation

In bridge construction, cables serve as essential tension elements, particularly in cable-stayed, suspension, and arch bridges, where structural performance relies heavily on their axial stiffness and dynamic behavior to enable long spans and efficient load transfer. Wang et al.[1] investigated the transverse seismic response of a medium-span cable-stayed bridge, highlighting the critical contribution of stay cables to lateral stiffness and energy dissipation under earthquake loading. Similarly, Galvín and Domínguez[2] demonstrated that the dynamic behavior of cables significantly affects vibration modes and damping characteristics in cable-supported systems, while Xiong et al.[3] extended these findings to super long-span bridges, proposing carbon fiber–reinforced polymer (CFRP) components as an effective solution to reduce self-weight and improve global efficiency. Latest advances in the seismic design of cable-stayed bridges further emphasize the importance of cable vibrations under seismic actions, showing that cables can experience significant dynamic amplification, mode coupling, and stress reversals during earthquakes, as observed in full-scale monitoring studies.[4,5]

While steel stay cables (SSCs) remain the most widely adopted solution in practice, their performance is increasingly constrained as span lengths increase. These constraints include excessive sag under self-weight, high fatigue sensitivity under cyclic loading, and strong susceptibility to

corrosion in aggressive environments. Almansour[6] demonstrated that hybrid cable arrangements can improve global stiffness and reduce deflections in long-span bridges, while Li and Ou[7] identified fatigue as the dominant long-term degradation mechanism in steel tendons based on structural health monitoring data. Moreover, wind- and seismic-induced cable vibrations, together with coupled deck-cable dynamic interactions, further aggravate these vulnerabilities by increasing stress ranges and accelerating damage accumulation. These limitations motivate the exploration of alternative cable solutions to improve dynamic performance and long-term durability in modern cable-stayed bridges.[8–10]

Carbon fiber-reinforced polymer (CFRP) cables offer a viable alternative due to their high strength-to-weight ratio, robust fatigue performance, and inherent corrosion resistance.[11–14] Liu et al.[12] detailed their mechanical advantages over steel in harsh environments, while Long et al.[13] showed improved aerodynamic behavior under dynamic wind loading. Recent developments in anchorage systems and long-term creep durability confirm the practical viability of CFRP in real-world bridge applications.[11,14]

Full-scale observations and refined numerical investigations[4] further suggest that stay-cable vibrations cannot always be regarded as purely local phenomena, because cable dynamics may interact with the global seismic response through modal coupling. Detailed field-based studies have shown that the dynamic spectrum of a cable-stayed bridge may include not only "pure structural" modes and "pure cable" modes but also mixed modes in which deck/tower motions coexist with in-plane and out-of-plane cable oscillations. Under these conditions, the activation of cable modes may contribute a non-negligible generalized mass, and when cable frequencies fall within (or close to) the dominant structural frequency range, cable motion can excite or amplify deck response and alter the distribution of modal mass participation. This coupling is particularly critical under earthquake excitation, as it may trigger significant dynamic amplification, mode interaction, and even stress reversals in the stays, with implications for both demand- and fatigue-sensitive components. Therefore, clarifying how the stay system participates in the overall dynamic response and how this participation changes when cable stiffness and mass are modified is a key motivation for the present study, which compares SSC, CFRP, and novel hybrid stay cable (HSC) solutions to assess their influence on global modal properties and the bridge's seismic response.

To overcome the limitations of steel and CFRP cables, the research community explores innovative solutions that leverage the advantageous material properties of both materials in the form of HSCs[15–17] by strategically combining steel and CFRP within a single hybrid wire strand (HWS) to achieve optimal performance. This strategy addresses the cost concerns associated with relying solely on CFRP, mitigates the vulnerabilities inherent to CFRP, and offers the potential to improve the thermal response of the bridge by using the high-strength steel coat. However, the current body of research on the actual real-time production of HSCs and their further application in civil structures, particularly in cable-stayed bridges, remains limited to theoretical ideas and design.[12,18,19] This scarcity underscores the need for further research in this area.

Scope of the work

Motivated by the promising potential of hybrid cable systems, this paper presents the experimental development and structural assessment of novel HSCs in cable-stayed bridges under seismic loading. These novel cables were developed within the framework of the European project FIRST-WIRE (FIber-Reinforced STeel WIRE; https://firstwire.eu/), which aims to introduce the use of these new hybrid cables in civil and industrial constructions. This project not only addresses the technical challenges encountered during the manufacturing and testing phases but also investigates the feasibility of implementing these hybrid cables in real structural applications.

The present paper analyzes the seismic performance of a pedestrian cable-stayed bridge equipped with HSC cables. In this respect, a comprehensive experimental and numerical evaluation was conducted, focusing on the mechanical characterization of the novel HSC cables and the structural performance of the bridge under earthquakes. The paper is articulated as follows. Section 2 outlines the mechanical characteristics of the tested full-steel and hybrid cables. Section 3 introduces the selected case study of bridge, detailing its configuration, stay cable arrangement, and construction stages analysis. Finally, Section 4 presents a comparative performance assessment of the bridge equipped with steel, CFRP, and hybrid cables both in construction and seismic conditions, along with the effect of corrosion on the SSCs and HSCs, highlighting the structural benefits and limitations of the proposed hybrid cable solution.

Mechanical Characterization of HWSs and Hybrid Cables

The following section introduces the novel hybrid wire and cable. Since a hybrid cable consists of multiple HWSs, it is important to thoroughly identify the key aspects of a single strand of the hybrid wire. Therefore, for both HWS and HSC, the mechanical behavior is examined using finite element modeling and experimental testing.

Fig. 1 illustrates the conceptual design of the proposed hybrid wire and the two corresponding hybrid cable configurations that can be derived from it.

The first type, the open spiral strand (OSS), is formed by helically twisting multiple hybrid wires around a central king wire. This configuration is characterized by its flexibility, ease of fabrication, and suitability for applications where moderate compactness and load uniformity are acceptable. The second type, the fully locked coil (FLC), is fabricated by adding one or more outer layers (two in this study) of interlocking Z-shaped steel wires. This design yields a more compact cross-section, higher axial stiffness, enhanced corrosion resistance, and a smoother external surface, all

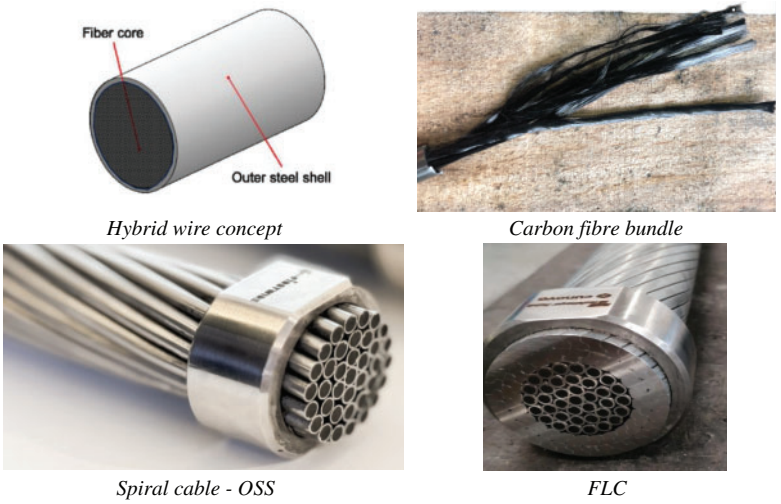

Figure 1. Hybrid wire and cable samples. FLC, fully locked coil; OSS, open spiral strand

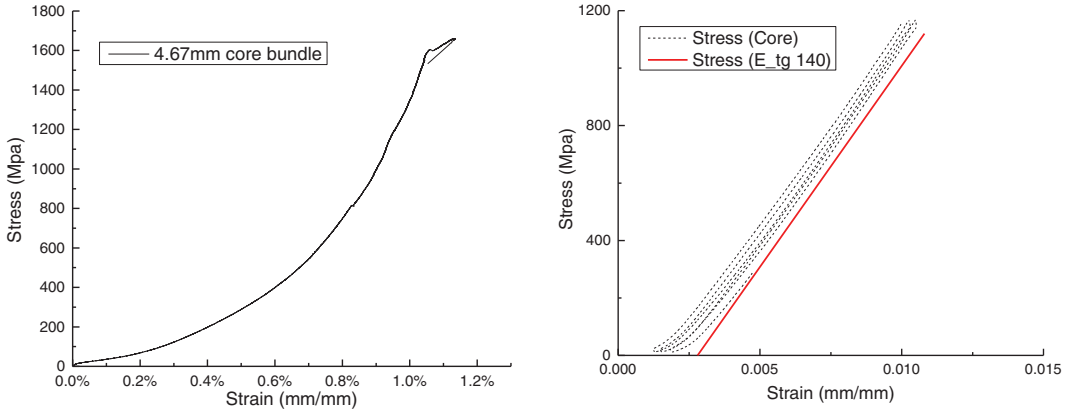

Figure 2. Breaking test results on 4.67 mm bundle (left), carbon bundle stress–strain response under cyclic loading (right)

of which are beneficial for both aerodynamic stability and anchorage interactions.

The long-term performance of SSCs is limited by fatigue and, more critically, by corrosion, which leads to progressive loss of cross-sectional area, stiffness, and structural capacity. On the other hand, CFRP cables offer excellent corrosion resistance and very high tensile strength, but their practical application is constrained by high material costs, brittle failure behavior, and complex anchorage systems that require specialized, often non-standard solutions. HSCs, based on HWSs combining a CFRP core with a stainless-steel external sleeve, have been proposed to overcome these limitations. In this configuration, the CFRP core provides high specific strength and corrosion resistance, while the steel shell ensures ductility, mechanical protection, and compatibility with conventional anchorage systems. Compared to full steel cables, HSCs exhibit good durability and reduced sensitivity to corrosion due to the presence of the CFRP core. Compared to pure CFRP systems, they offer robustness, simpler installation, and lower overall costs while maintaining high tensile capacity. This hybrid solution, therefore, represents a technically and economically viable compromise among performance, durability, and constructability for real-world bridge applications.[13,14]

Mechanical properties of the hybrid wires

This section introduces the concept of novel hybrid wires, with a primary focus on their mechanical properties and design parameters. The hybrid wire has a high-performance stainless-steel outer shell (3–5 mm outer diameter, 0.3–1.0 mm thickness) that shields a high-performance internal carbon fiber core obtained by twisting different tows of 12k/24k filaments.

Fig. 2 shows the load vs. displacement and stress vs. strain behavior for the carbon bundle. Here, the stresses were calculated by dividing the force recorded during the test by the nominal inner area of the steel tube, and not to the net area of the filaments. Fig. 2 (left) illustrates the outcomes of a test conducted to derive the ultimate strength of the carbon bundle. The results demonstrate that stresses exceeding 1600 MPa can be attained. Fig. 2 (right) depicts the outcomes of a subsequent test in which the carbon bundle was subjected to cyclic loading with the objective of determining the elastic modulus and any alterations therein. Apart from an initial phase of fiber settlement, the results demonstrate that a modulus of 140 GPa is consistently attained over a broad range of stresses. Fig. 3 shows the tensile behavior of an

empty 6Mo stainless-steel tube (5.16 mm × 0.4 mm) used for hybrid wire manufacturing.

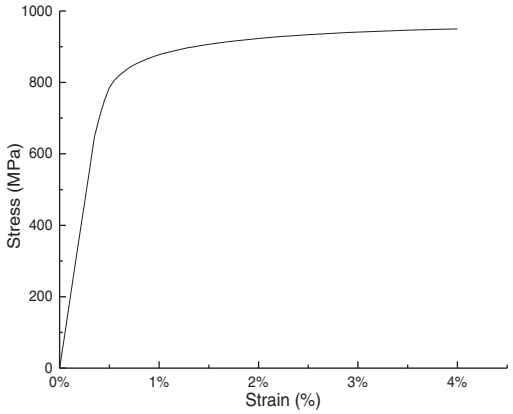

Figure 3. Tensile response of 6Mo stainless-steel tube of dimension 5.16 mm × 0.4 mm

In Fig. 4 the load–displacement curves of 5.16 and 3.51 mm hybrid wires are shown. The obtained failure loads correspond to tensile strengths of approximately 1430 and 1650 MPa for the 5.16 and 3.51 mm wires, respectively. In the present set of hybrid wires, the volume ratio of the CFRP core ranges from 57% to 72%, consistent with existing literature findings. The volume ratio is 55% for short lengths and 85% for long lengths.[15]

The theoretical behavior of the hybrid wire is modeled by superimposing the contributions of the external stainless-steel tube and the internal carbon fiber bundle. To determine the composite stress–strain response, it is assumed that both materials experience the same axial deformation, that is, strain compatibility is imposed between steel and CFRP. This assumption is valid within the elastic regime and is supported by pull-out tests conducted during the project, which revealed a tangential frictional stress of approximately 8 MPa at the steel–CFRP interface. Such a level of interfacial resistance is sufficient to prevent slippage beyond a short distance from the wire ends, ensuring that the two components act in unison. Accordingly, the axial force of the hybrid wire can be calculated as the sum of the individual contributions of steel and CFRP, as defined in Eq. (1),

$$\begin{aligned} \varepsilon_{hybrid} &= \varepsilon_{core} = \varepsilon_{tube} \\ F_{hybrid} &= F_{core} + F_{tube} \end{aligned} \tag{1}$$

From the above conditions, for any applied strain ε_{hybrid}, and given the individual stress–strain response of the core and the tube, which can be obtained experimentally, we can calculate the force contribution for the two single components simply as

$$\begin{aligned} F_{core} &= \sigma_{core} \cdot A_{core} \\ F_{tube} &= \sigma_{tube} \cdot A_{tube} \end{aligned} \tag{2}$$

An equivalent stress in the hybrid component is thus obtained by dividing the total force by the gross cross-sectional area; see Eq. (3). It provides a homogenized measure for characterizing the global response of the hybrid section. The actual force contribution of the tube and fiber core is governed by their respective axial sectional stiffnesses (element analysis [EA]), and the assumption of strain compatibility ensures a consistent deformation.

$$\sigma_{hybrid} = (F_{core} + F_{tube})/A_{hybrid} \tag{3}$$

As an intermediate step toward modeling the full hybrid rope, we conducted a series of FE analyses (FEAs) for a single wire subjected to tensile loading. The adopted model is shown in Fig. 5. The analyses were performed using the FE software ABAQUS,[20,21] following the implicit solution scheme. The mesh was created using 8-node solid continuum elements C3D8. The two regions of the wire with different materials were modeled considering the mesh as continuous. In the model, different properties are assigned to the steel surface elements and the carbon fibers. An elastic-plastic behavior was assigned to the tube based on test results, while a linear elastic behavior was used for the carbon fibers with a modulus of 140 GPa. The hybrid tensile strength exceeding 1400 MPa, despite individual constituent strengths being lower, reflects the optimized force-sharing between CFRP

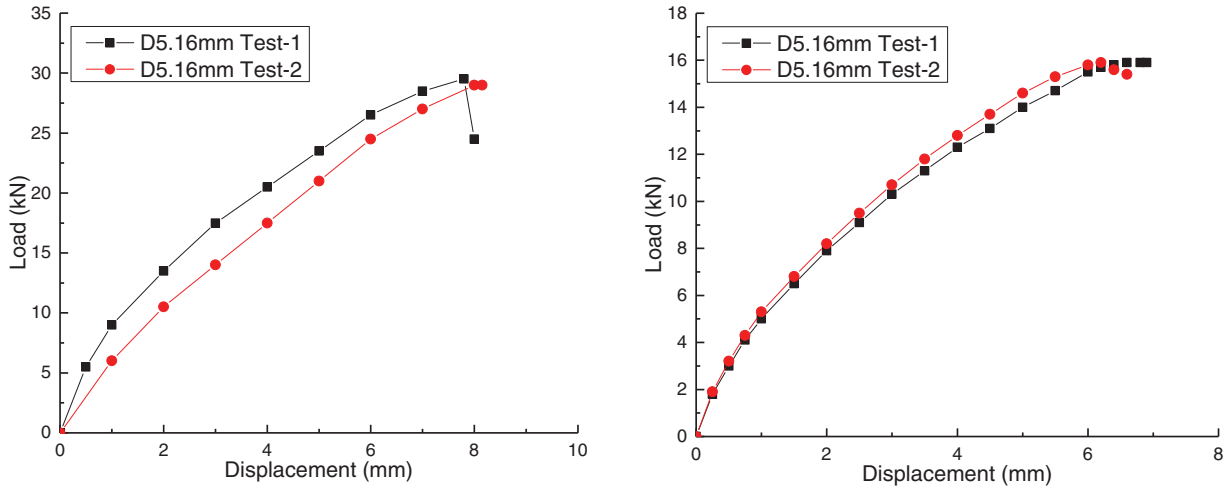

Figure 4. Tensile specimen and test results: 5.16 mm diameter (left) and 3.51 mm diameter (right)

and steel under strain compatibility. Since CFRP contributes significantly to the axial stiffness and force at relatively lower strain, the total axial force reaches high values. The σ_{hybrid} value is the nominal stress normalized to the gross area, which is not indicative of the local peak stress in either material.

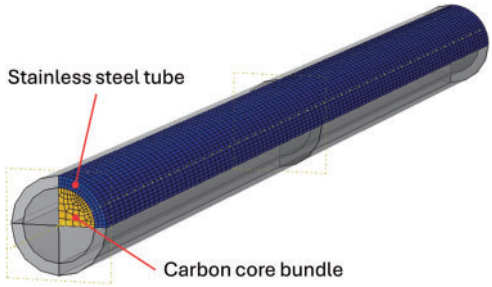

Figure 5. Finite element (FE) model of a hybrid wire

It is essential to note that, although the CFRP and stainless-steel components exhibit comparable ultimate tensile strengths (~1400–1600 MPa), they differ substantially in their ultimate strain capacities. CFRP typically fails at a much lower strain (~1%–1.5%) compared to stainless steel (~10%–15%). In the hybrid configuration, the CFRP core is expected to fracture first, as it reaches its ultimate strain earlier under axial loading. Meanwhile, the surrounding steel tube continues to deform, typically entering the elastic–plastic regime but not necessarily reaching its own strain limit. In the analytical model, this mismatch in strain capacity is accounted for by applying a strain–compatibility assumption, which assumes that both materials experience the same axial strain up to the point of CFRP fracture. This is a valid approximation in the pre-fracture phase, owing to high interfacial friction that prevents differential slip between the components. After CFRP rupture, however, the system transitions to a different load-bearing mechanism, dominated by the residual capacity of the steel shell. The post-fracture behavior of the steel shell falls outside the scope of the current study and will be investigated in future work focused on progressive failure and fatigue endurance.

Fig. 6 (left) shows a good match between the analytical and numerical results for a 3.51 mm hybrid wire under tensile loads. Typically, the stress–strain behavior of the hybrid wire exhibits two distinct regions, corresponding to the elastic moduli E1 and E2, of approximately 150 and 75 GPa. The transition knee is attributed to the tube's yielding, which reduces the stiffness of the hybrid wire. Fig. 6 (right) shows the FE model (FEM) strain–stress curves obtained for a wire diameter ranging from 3.31 to 5.47 mm. The behavior appears very similar, except after the post-yielding phase of the external steel coating, for which the smallest wires exhibit a reduced E2.

In Fig. 6, the apparent yield point observed for the CFRP core at approximately 600 MPa does not correspond to fiber rupture, but rather to the onset of matrix cracking and interfacial degradation between the CFRP core and the surrounding steel tube under combined axial and torsional loading. This stress plateau results from a partial reduction in load-transfer efficiency caused by local damage within the polymer matrix and at the composite interface, a common occurrence in hybrid multi-material systems. The CFRP fibers maintain structural integrity and contribute to the global resistance of the hybrid wire up to their ultimate tensile capacity, which exceeds 1400 MPa in direct uniaxial tensile tests. Therefore, the observed stress limitation reflects interfacial and matrix-controlled behavior rather than intrinsic failure of the CFRP material.[17]

Characteristics of the hybrid cables

Various combinations of hybrid wires can be used to create a hybrid cable. An FLC configuration is typically employed for cable-stayed bridges. This configuration consists of a core of open spiral hybrid wires, which are then locked by one or two layers of Z-steel strands, as shown in Fig. 6. The FLC cable is chosen for both the FEA and experimental testing presented in this paper. A model of a 60 mm hybrid FLC rope has been set up by adopting the commercial software ABAQUS.[22] The model mesh is shown in Fig. 6, which consists of a rope section with a length of 6 times the diameter.

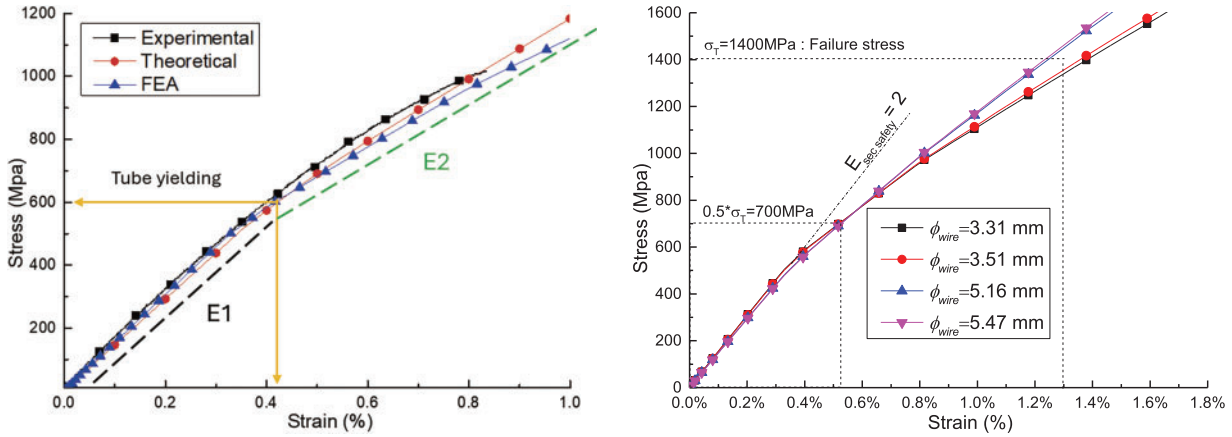

Figure 6. Experimental vs. numerical comparison for a 3.51 mm wire (left); finite element analysis (FEA)-estimated tensile behavior of hybrid wires under tensile load predicted by FEA (right)

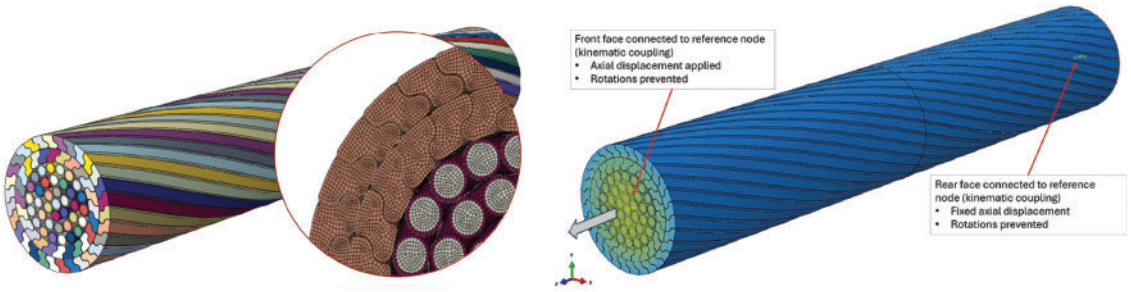

Figure 7. Fully locked coil (FLC) cable finite element (FE) model with its mesh projection and boundary conditions applied to the FE model of the FLC rope

The wires were modeled using 3D solid strain elements of the C3D8 type. In particular, each hybrid wire was modeled as a single entity, and different materials were assigned to the regions representing the bundle and the outer steel tube. In this way, the condition of a strong bond between the core and the tube is simulated. Frictional contact between wires was modeled using the coulomb friction model with coefficient f = 0.1. To model the hybrid wire in Abaqus, boundary conditions were applied using reference points at the wire ends. One end of the wire was fixed to prevent rotation but allowed to move axially. The other end was subjected to a controlled axial displacement to simulate tensile loading. These boundary conditions help replicate the loading of cables in real structural applications. Because of the complex interactions and contact between individual wires within the hybrid structure, the explicit solver in Abaqus was used to ensure numerical stability during large deformations. Additionally, mass scaling was applied to reduce the total simulation time while maintaining accuracy. A sensitivity analysis was performed to select an appropriate mass scaling factor, ensuring that the artificial increase in kinetic energy did not compromise the quality of the results.

Various full-scale experimental tests (breaking tests) were conducted to validate the mechanical behavior of the hybrid FLC cable and to confirm the reliability of the numerical model. As shown in Fig. 8, the full-scale sample consisted of a 60 mm diameter FLC cable equipped with a specially designed socketing system. This system uses steel cylinders filled with resin, into which the wire ends are partially uncoiled and bent into an S-shape to enhance mechanical interlock and friction. This configuration proved effective in preventing slippage or premature failure at the terminations, thereby ensuring the cable's integrity during high-load testing.

The specimen had a free length of approximately 4.20–4.30 m and a total length of about 5.00 m. Experimental results confirmed strong tensile performance, with the system reaching loads equivalent to around 1400 MPa of tensile strength, calculated over a net cable cross-sectional area of 2460 mm^2. However, it is important to note that the FEA conducted in this study does not model the socketing system. The FEA focuses solely on the internal stress and strain behavior of the hybrid cable. As shown in Fig. 9, there was a strong agreement between the experimental load-strain response and the FEA results throughout the entire loading

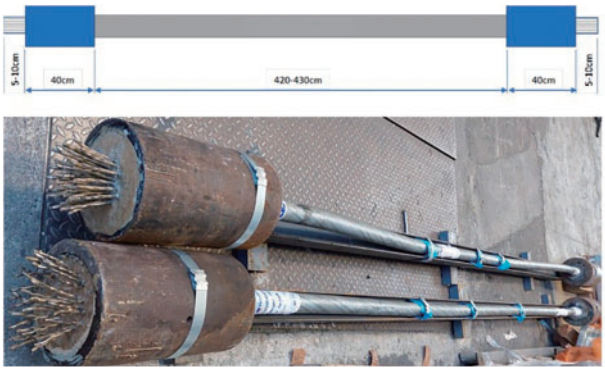

Figure 8. Axial breaking tests samples configuration

phase. This supports the validity of the developed numerical model in accurately simulating the mechanical performance of hybrid cable systems.

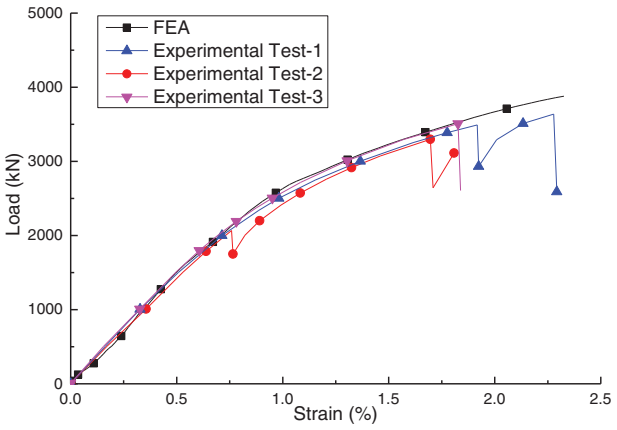

Figure 9. Comparison of experimental and numerical results of the hybrid fully locked coil (FLC) cable. FEA, finite element analysis

These values confirm that hybrid cables exhibit high stiffness and tensile strength suitable for structural applications, with FLC configurations offering the best mechanical performance. Table 1 presents the primary mechanical properties of OSS and FLC with two-layer Z-shaped cable configurations. Based on experimental and numerical analyses, the elastic modulus of hybrid cables varies depending on

Table 1. Mechanical properties of hybrid cable

Type of cable configuration	Diameter (mm)	Max breaking load (kN)	Elastic modulus (GPa)	Axial stiffness (MN)	Linear mass (kg/m)	Source
1. Spiral (OSS)	35.5	1017	114	88.52	2.93	Test
2. Fully locked coil with single Z cable layer (FLC)	48	2117	116.98	177.37	8.75	FEA
3. Fully locked coil with dual Z cable layer (FLC)	60	3501	120.85	297.03	16.41	Test

Note: FLC, fully locked coil; OSS, open spiral strand.

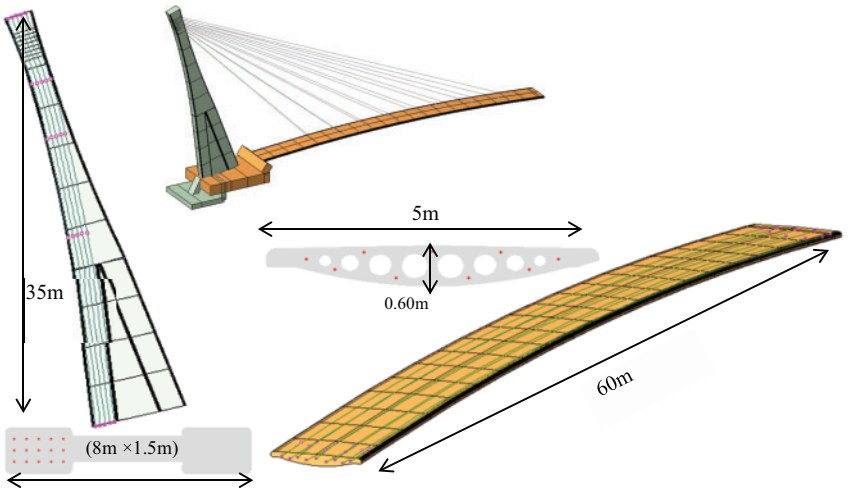

Figure 10. Design details of bridge: deck section and tower section (all units in m)

their construction: spiral (OSS) cables (∅35.5 mm) demonstrated an elastic modulus of 114 GPa with a breaking load of 1017 kN. FLC with single Z-layer (∅48 mm) showed a modulus of 116.98 GPa, reaching a load capacity of 2117 kN. FLC with dual Z-layer (∅60 mm) reached the highest modulus of 120.85 GPa and a maximum breaking load of 3501 kN.

Description of the Case Study

Description of the cable-stayed bridge geometry and material

The case study analyzed herein is a pedestrian bridge in Italy designed for cyclists and pedestrians to cross. The total span of the bridge is 77 m, with a clear span of 60 m. The deck depth of the bridge is 0.64 m, whereas the maximum width of the deck is 4.88 m. Fig. 10 shows the bridge profile of the present study. Both the deck and tower sections are made of prestressed concrete. The prestressed concrete deck is equipped with nine steel tendons, whose main sections are illustrated in Fig. 10. The deck is built by using three temporary supports. After that, the prestressing system in the deck is posttensioned. Similarly, the tower is made of prestressed concrete with 15 prestressing strands, as shown in Fig. 10.

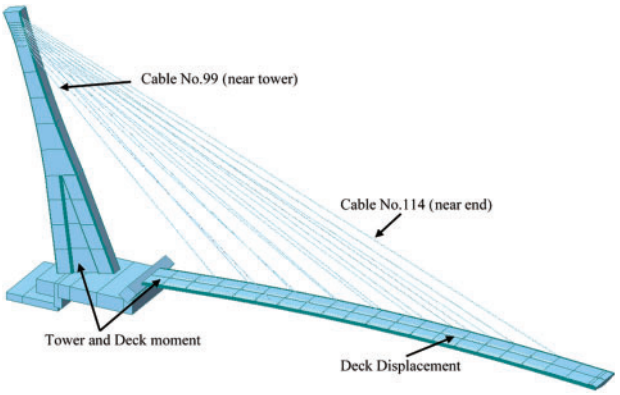

Figure 11. Three-dimensional finite element (FE) model of the bridge

The three-dimensional (3D) FEMl of the bridge, built in MIDAS Civil, is illustrated in Fig. 11. A 3D FEM of the cable-stayed pedestrian bridge (60 m main span) was developed in MIDAS Civil. The model includes the pylon, deck, and stay cables to accurately capture global stiffness, load distribution, and pre-tensioning effects. The tower is inclined at 20° from the vertical. The pylon is modeled using 18 tapered beam elements (38 nodes). Its cross-section tapers from 8 m at the base to 2 m at the top, with a constant thickness of 1.5 m. It is vertically posttensioned with 15 steel

cables. The deck is a lightweight concrete deck spanning 60 m and modeled with 22 beam elements (29 nodes). It includes nine internal prestressing tendons aligned longitudinally. The 16 stay cables (8 symmetric pairs) present in the bridge are modeled as truss elements. They vary in length from 42 m to approximately 80 m and are inclined between 24° and 45°. Steel cables have a 37 mm nominal diameter, while hybrid cables are 48 mm in diameter. The complete model consists of 85 nodes and 67 elements, with cable and tendon pretension modeled using dedicated elements to simulate realistic stress transfer and behavior. Materials and sectional properties of the deck and tower are reported in Table 2. All supports are modeled as fixed in the global system. However, to allow for the effects of prestressing in the deck, the support located at the deck's far end (opposite the tower) is not fully restrained. Instead, it is connected to a secondary fixed support through rigid links that allow free movement in the longitudinal (x) direction and permit rotation around the x- and y-axis. This setup enables the prestressing tendons to induce axial compression without generating unintended restraint forces at the far support, ensuring a realistic simulation of deck deformation.

Description of the stay cables and construction stage analysis

The bridge was originally designed with SSCs. However, to compare their performance with that of the proposed cable, a solution with HSCs is also considered. The material characteristics and diameter of both cable types are given in Table 3. Three models of the same bridge were constructed, each with a different type of cable. The steel cables used are the same as those used for the construction of the original bridge design, while for the HSC it was decided to use full-locked coils with a CFRP core and an external steel layer composed of wires with a Z-shaped section. As for the full-CFRP cables, ropes made with 37 CFRP wires from Tokyo Rope were used. The stays are arranged in two converging planes so that the bridge can be classified as asymmetrical side-suspended, as shown in Fig. 11. The shortest cable has a length of 42 m, whereas the longest cable is 80 m. The angles of attack with the deck vary from a minimum of 24° to a maximum of 45°. The connection between the stay cable and the deck, as well as between the tower and the stay cable, is created in the numerical model by using rigid links.

The replacement of SSCs with HSCs in the bridge design was primarily governed by equivalent ultimate tensile capacity. This ensured that structural safety was maintained, with a density less than half that of the SSCs, which benefits weight reduction and improves corrosion resistance. However, although the stiffness of the hybrid solution is lower, this was acceptable given the short span nature of the pedestrian bridge and the minimal effect on global displacement.

The assessment of the initial stress level in the cables for the subsequent seismic analysis has been conducted through the unknown load method. This method facilitates the determination of unknown load factors for each stay

Table 2. Material and sectional properties of cable-stayed bridge

	Parameter	Symbol	Unit	Value
Tower concrete- (C45/55)	Elastic modulus	E_t	GPa	36.28
	Weight density	ρ_t	kN/m^3	25
	Poisson's ratio			0.2
	Moment of inertia	I_{xx}	m^4	1200
	Cross-sectional area (top)	$A_{T\text{-}Top}$	m^2	7.24
	Cross-sectional area (bottom)	$A_{T\text{-}Bottom}$	m^2	10.25
Deck concrete- (C45/55)	Elastic modulus	E	GPa	36.28
	Cross-sectional area	A	m^2	2.33
	Weight density	ρ_t	kN/m^3	25
	Poisson's ratio			0.2
	Bending moment of inertia	I_{yy}	m^4	0.0584
	Torsional moment of inertia	I_{xx}	m^4	0.213

Table 3. Material properties of stay cables

Type of cable material	Modulus of elasticity (GPa)	Poisson ratio	Density (kN/m^3)	Diameter of cable (mm)
Hybrid	117	0.3	47.87	48.46
Steel	165	0.3	81.95	37
CFRP	145	0.3	18.96	32

Note: CFRP, carbon fiber–reinforced polymer.

cable, considering initial dead load conditions in terms of pre-defined moment or displacement values. More details are provided in Hassan et al.,[23] Midas,[24] and Yu et al.[25] Fig. 12 illustrates the initial cable forces for the present case study for the SSC, CFRP, and HSC cases. Furthermore, the forward construction stage analysis (F-CSA) methodology was considered to determine the cable forces during the several phases of the bridge erection. The construction stages for the selected case study are presented in Table 4.

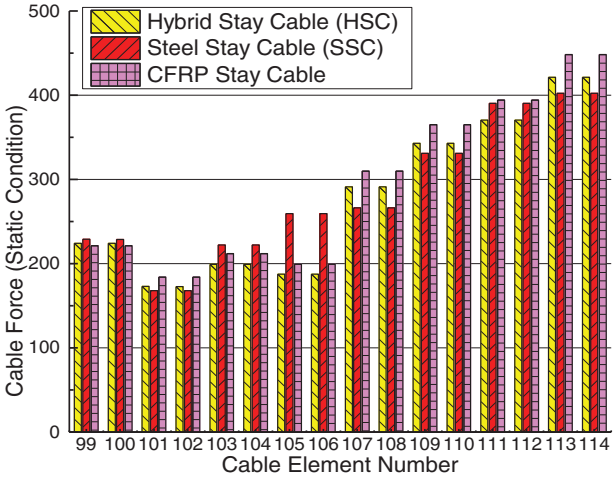

Figure 12. Initial stay cable forces for cable-stayed bridge. CFRP, carbon fiber–reinforced polymer; HSC, hybrid stay cable; SSC, steel stay cable

Fig. 13a shows the cable forces in the several construction stages. The stay cable forces near the end supports exhibit a constant trend when HSCs are used, whereas the steel cable forces increase during construction. Since the cables positioned near the tower are relatively short, their axial deformation under load is minimal. As a result, the stiffness requirements for these short cables can be satisfied with both steel and hybrid materials without a significant difference in the applied tension. In other words, due to the limited length, the total elongation is small, and both cable types (steel and hybrid) require nearly the same pull force to achieve the prescribed displacement and maintain the deck geometry as per design. This 3% change between CS-6 and CS-7 (final construction stage) represents a benefit, as the force distribution in the HSCs appears well controlled from the beginning of the construction phase. Similar results can also be found in the literature.[26] It is important to note that the stay cable becomes active starting from the fourth construction stage, as shown in Fig. 13a.

The deck moment increases from the construction stages 3–5 for both the cable types, as shown in Fig. 13b, which is due to the tensioning of the stay cables and the prestressing of strands in both the tower and deck. It is interesting to note that, in CS-7, the vertical displacement of the tower and deck increases, whereas the absolute moment of the deck (M_y) decreases.

This is mainly due to the removal of the temporary deck supports in CS-6, which activated the significant flexibility of the longest-stay cables. Table 5 presents the response quantities of interest (QoI), such as tower and deck vertical displacements and bending moments, for the different CSs.

Seismic Analysis of the Bridge Equipped with HSC and SCC

Dynamic characterization of the bridge

A modal analysis has been carried out to understand the dynamic properties of the cable-stayed bridge. Table 6 shows the first 10 natural frequencies of the cable-stayed bridge. It can be seen from the table that the frequencies of the cable-stayed bridge equipped with the HSCs are slightly higher than those of the SSCs. From a material perspective, the increase in natural frequency is attributed primarily to the lower mass density of CFRP compared to steel. The hybrid cables, featuring a CFRP core and a stainless-steel shell, achieve a significant weight reduction, approximately 40% lighter than full-steel cables.

A similar behavior have already been observed in the existing literature.[26,27] In general, the influence of hybrid cable mass in cable-stayed bridges with longer spans will require further investigation. It can be seen from Table 6 that frequencies for both cable-stayed bridge cases, particularly those in the range 5–7, exhibited notably different vibration mode orders.

This variation in the frequency distribution is illustrated in Fig. 14, which depicts the principal vibration modes of the bridge: Fig. 14a, first lateral bending mode of the tower; Fig. 14b, first vertical bending mode of the deck; Fig. 14c second vertical bending mode of the deck; Fig. 14d, combined bending mode of deck and tower; Fig. 14e, first lateral bending mode of the deck; and Fig. 14f, coupled lateral bending mode of the deck with vertical bending of the counterweight at the heel foundation. The differences in the sequence of these modes correspond to shifts in the modal mass percentage distribution across different directions for both configurations. Apart from this reordering of specific fundamental modes, the remaining vibration modes showed no significant deviations between the steel and hybrid cable cases.

The influence of cable material on the bridge dynamics can be interpreted through the axial stiffness $k_{ax} = EA/L$ and the corresponding cable mass. For the shortest stay (about 42 m), the axial stiffness is approximately 4.22 MN/m for SSC, 5.14 MN/m for HSC, and 2.78 MN/m for CFRP, while for the longest stay (about 80 m), it reduces to about 2.22 MN/m (SSC), 2.70 MN/m (HSC), and 1.46 MN/m (CFRP), highlighting the expected length dependency. In parallel, the stiffness-to-weight efficiency differs markedly among materials, since CFRP provides the highest specific stiffness (high E with very low density), whereas the HSC solution achieves higher EA primarily through a larger area and thus similar cable self-weight to steel. These combined stiffness and mass differences affect modal participation factors by modifying the effective modal mass and the relative share of strain energy stored in the stay system versus the deck and pylon. In practice, lighter cable systems reduce inertial

Table 4. Construction stage sequence and list of activities performed for the cable-stayed bridge

Construction stages	Activity
CS-1	The foundation and bridge tower are constructed in the first construction stage, which lasts 10 days.
CS-2	The supporting deck is completed in the second construction stage. It rests on five temporary supports 15 m apart and behaves like a continuous beam.
CS-3	In the third construction stage, the deck and prestressing cable tensioning are constructed when the minimum strength in the deck is gained. This construction stage is completed in 9 days: on the first day, concrete casting is done, and on the last day, prestressing action in the deck is performed once the minimum strength of concrete is reached.
CS-4	In the fourth construction stage, the stay cables are installed along with the first phase of prestressing the tower cables up to 40% of the maximum tension, T_{max} = 1350 MPa, and the first phase of tensioning the stay cables. This phase has a duration of 9 days; on the first day, the prestressing cables of the tower are performed at the top side to a magnitude of 540MPa, and on the remaining 8 days, one day at a time, the stay cables are tensioned in pairs by applying the loads identified by the unknown load method.
CS-5	In the fifth construction stage, the second phase of prestressed cables in the tower is stressed up to 70% of the maximum tension; also in this construction step, ballast is applied on the foundation at the tower side of the bridge. The total duration of this stage is 10 days; on the first day, the prestressed cables of the tower are provided an additional pull of 405MPa. On the next 8 days, one day at a time, the stay cables are stretched in pairs by applying the loads; and finally, on the last day, the ballast load is added.
CS-6	After the two stages of stressing the pretension cables in the deck and tower along with stay cables, the temporary supporting deck is removed in the sixth construction stage.
CS-7	The prestressed cables in the tower and stay cables are now stressed up to 100% of the designed strength. Like the fourth construction stage, this phase also lasts 9 days; on the first day, the tower's prestressed cables are provided with a final pull force of 405 MPa, and on the remaining 8 days, one day at a time, the stays are stretched in pairs by applying the loads.

Note: CS, construction stage.

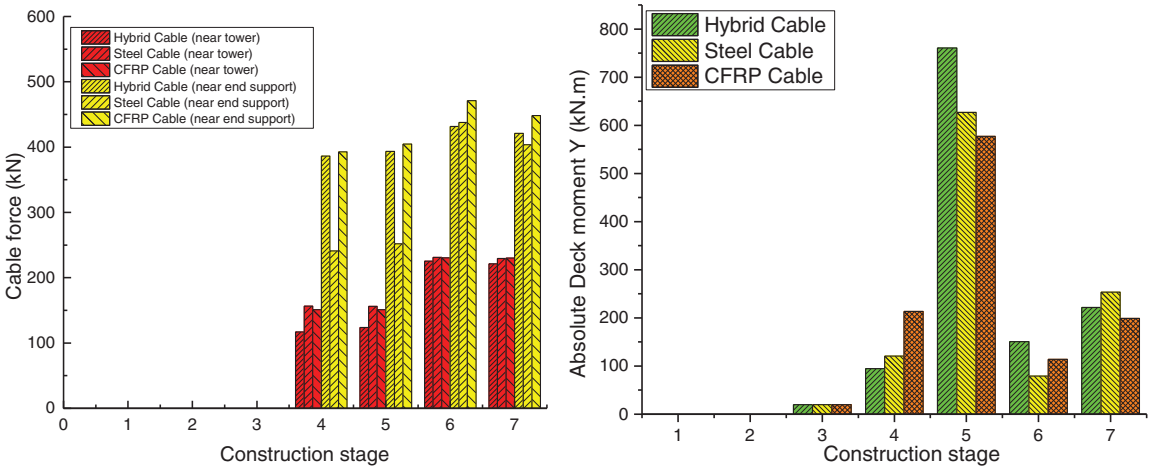

Figure 13. Comparison between the different stay cable materials at various construction stages for various response quantities of interests (a) cable force near the tower (cable no. 99) and cable force near end support (cable no. 114), and (b) absolute deck moment (My). CFRP, carbon fiber–reinforced polymer

contribution under seismic input and can shift participation toward higher-frequency content, while stiffer stays increase the constraint on deck deformation. This explains why the global mode shapes remain deck–tower dominated in this short-span bridge, yet small shifts in frequency content and energy distribution are observed when moving from SSC to HSC and CFRP configurations.

The record selection concerned the Amatrice city, well-known for the devastating earthquake that struck Central Italy in 2016. Amatrice is located in the Lazio Region

Table 5. Comparison between the different response quantities for different construction stages

Construction stage	Tower vertical displacement (m)			Tower bending moment (M_y) (kN.m)			Deck vertical displacement (m)		
	HSC	CFRP	SSC	HSC	CFRP	SSC	HSC	CFRP	SSC
1	0	0.000	0	−329.4	−329.45	−329.4	0	0	0
2	−0.004	−0.004	−0.004	−17901.1	−17901.06	−17901.1	0	0	0
3	−0.004	−0.004	−0.004	−17901.1	−18225.34	−17901.1	−0.019	−0.019	−0.019
4	−0.015	−0.010	−0.021	−62335.4	−42405.67	−76642.6	−0.018	−0.018	−0.018
5	−0.007	−0.009	−0.009	−35294.8	−37191.79	−37874	−0.045	−0.004	−0.038
6	−0.018	−0.017	−0.021	−81649.1	−65551.52	−84741	0.07	0.06	0.06
7	−0.028	−0.029	−0.03	−62334.1	−61357.04	−61603.3	0.091	0.08	0.103

Note: CFRP, carbon fiber–reinforced polymer; HSC, hybrid stay cable; SSC, steel stay cable.

Table 6. The first 10 natural frequencies of the bridge for different stay cable material

Mode number	Frequency (Hz)			Translation-X			Translation-Y			Translation-Z		
				mass (%)			mass (%)			mass (%)		
	SSC	CFRP	HSC	SSC	CFRP	HSC	SSC	CFRP	HSC	SSC	CFRP	HSC
1	0.952	0.926	0.957	–	0.26	–	10.26	–	10.32	–	7.14	–
2	1.013	0.963	1.108	0.36	–	0.48	–	10.18	–	6.89	–	6.58
3	1.879	1.747	2.075	0.4	0.3	0.51	–	–	–	0.31	0.32	0.27
4	3.107	3.039	3.246	0.31	0.23	0.37	–	–	–	0.87	0.98	0.77
5	3.951	3.731	**4.253**	6.17	6.23	–	–	–	5.18	2.57	2	–
6	4.239	4.261	**4.326**	–	–	6.07	6.12	6.75	–	–	–	28.62
7	4.326	4.326	**4.374**	6.89	6.87	7.08	–	–	–	27.58	27.7	2.04
8	4.392	4.429	4.455	–	–	–	6.44	5.75	7.33	–	–	–
9	4.577	4.577	4.577	–	–	–	33.79	33.88	33.79	–	–	–
10	4.964	4.940	5.049	0.02	0.03	–	–	–	–	0.05	0.03	0.09

Note: CFRP, carbon fiber–reinforced polymer; HSC, hybrid stay cable; SSC, steel stay cable.

(Italy), with latitude (ED50) 42.6274°, and longitude (ED50) 13.2836°, and soil type B. For the present study, 30 earthquake records are used with return periods of 2475 years, with a probability of occurrence in 50 years of 2%. The response spectrum of selected ground motions is shown in Fig. 15. More details on the selection of the natural records can be found in Giannini et al.[28]

Time history analysis and seismic response characterization

This section presents the bridge's seismic response. The seismic input consists of three-directional ground motion records applied simultaneously: the major component is aligned longitudinally with the bridge deck (global X-direction), the minor component is transverse to the deck (global Y-direction), and the third component is vertical (global Z-direction). This setup replicates realistic seismic excitation and captures interactions among the bridge's longitudinal, transverse, and vertical responses. We compare both stay cable solutions through a time-history analysis to identify significant differences and variations. It involves various response QoI, including the tower's displacements at the top, the moment of the tower and deck, deck vertical displacement, and cable forces in the shortest and longest cables. The locations where the QoIs were measured are shown in Fig. 11.

For tower lateral displacement (Fig. 16a), all cable systems display similar peak values: 0.2125 m for SSC, 0.2128 m for HSC, and 0.2164 m for CFRP. This indicates that the cable material has minimal influence on the lateral flexibility of the tower. In contrast, vertical deck displacement and internal moment responses show more variation. As seen in Fig. 16b, the CFRP system reaches the highest vertical displacement (0.113 m), followed by SSC (0.099 m) and HSC (0.091 m). CFRP cables have lower axial stiffness, which makes them more flexible under tension. However, because they are much lighter, their stiffness-to-weight ratio is high, meaning they generate less inertial force during seismic motion. This helps control dynamic responses despite their

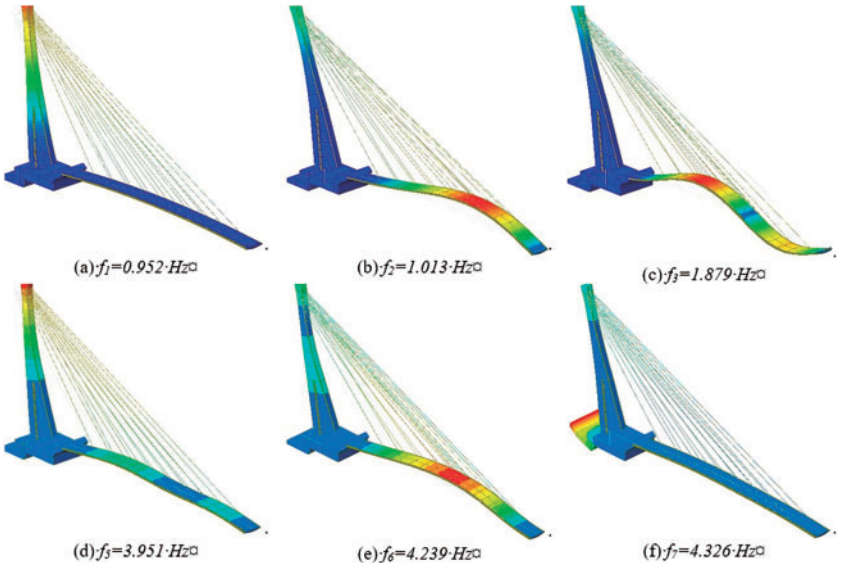

Figure 14. Different modes of vibration for the full steel cables bridge

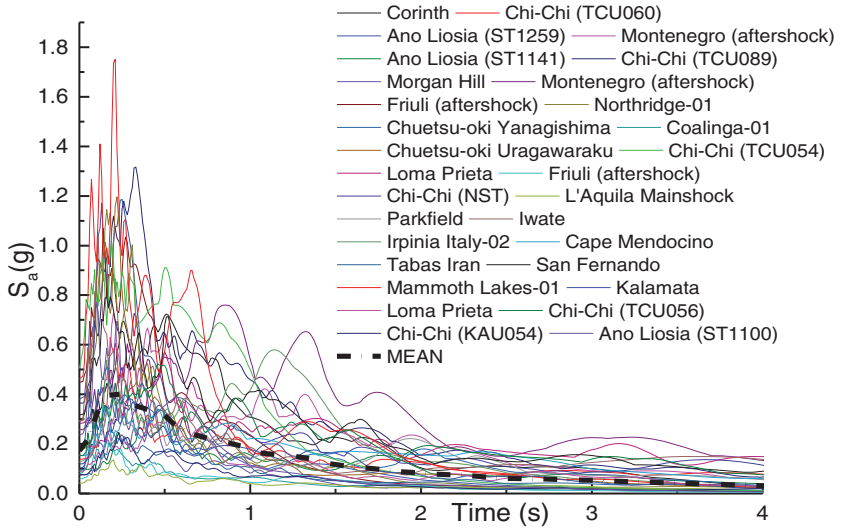

Figure 15. Response spectra of the ground motions

flexibility. In terms of tower moment My (Fig. 16c), the SSC system exhibits a peak of 69026 kN.m, with HSC at 68571 kN.m and CFRP at 67865 kN.m. While the peak magnitudes are similar, both CFRP and HSC systems exhibit a noticeable phase shift in their time–history responses. This is primarily due to their lower mass, which alters the natural frequencies and vibration behavior of the structure. Deck moment My (Fig. 16d) is consistently higher in the SSC system, especially at lower and higher PGA levels. This reflects the increased dynamic amplification associated with more flexible cables. The HSC and CFRP systems reduce the peak moment demand, improving overall dynamic performance not by increasing static stiffness but by influencing modal properties and reducing the bridge's inertial response.

Fig. 17 illustrates the time–history of cable tension for three different cable types. In Fig. 17a, which represents the cable near the tower, all systems (SSC, HSC, and CFRP) exhibit similar fluctuation patterns, with only minor differences in peak values. In contrast, Fig. 17b, which corresponds to the longer cable near the end support, reveals a much higher and more stable tension in the CFRP cables throughout the excitation. This is primarily due to their higher initial static tension, which stems from the higher tensile strength and reduced elastic elongation of CFRP. Additionally, CFRP's high strength-to-weight ratio enables it to resist dynamic effects more effectively, resulting in a consistently elevated force level. The SSC and HSC cables show lower average tensions and more scattered fluctuations. These results suggest that material selection significantly influences axial force behavior, especially for longer cables, highlighting the need for further investigation into tension control, anchorage detailing, and long-span applications when CFRP is used.

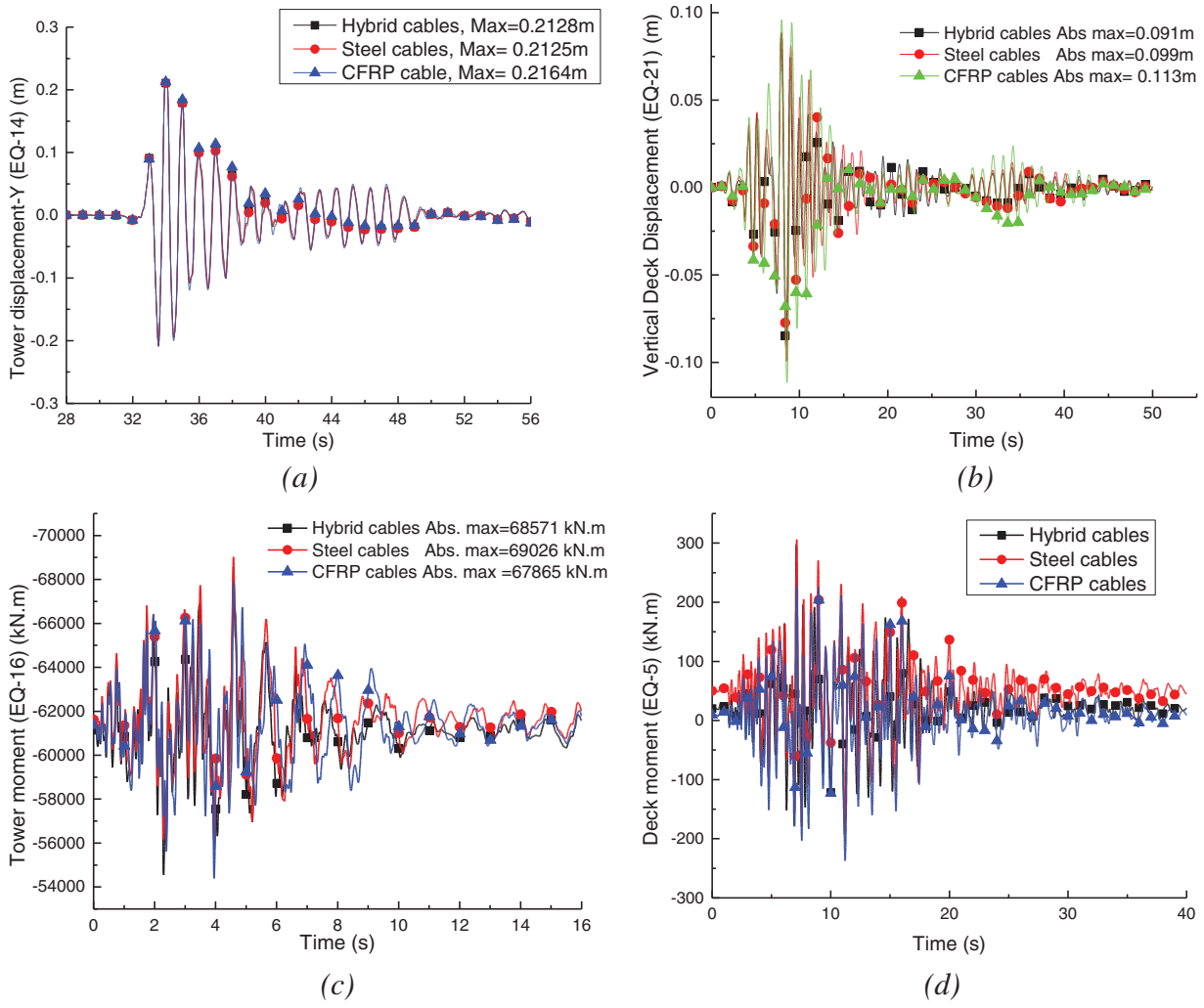

Figure 16. Time–history plots of various response quantities of interest for the tower: (a) tower lateral displacement, (b) deck vertical displacement, (c) tower bending moment (M_y), and (d) deck moment (M_y). Abs, absorbance; CFRP, carbon fiber–reinforced polymer

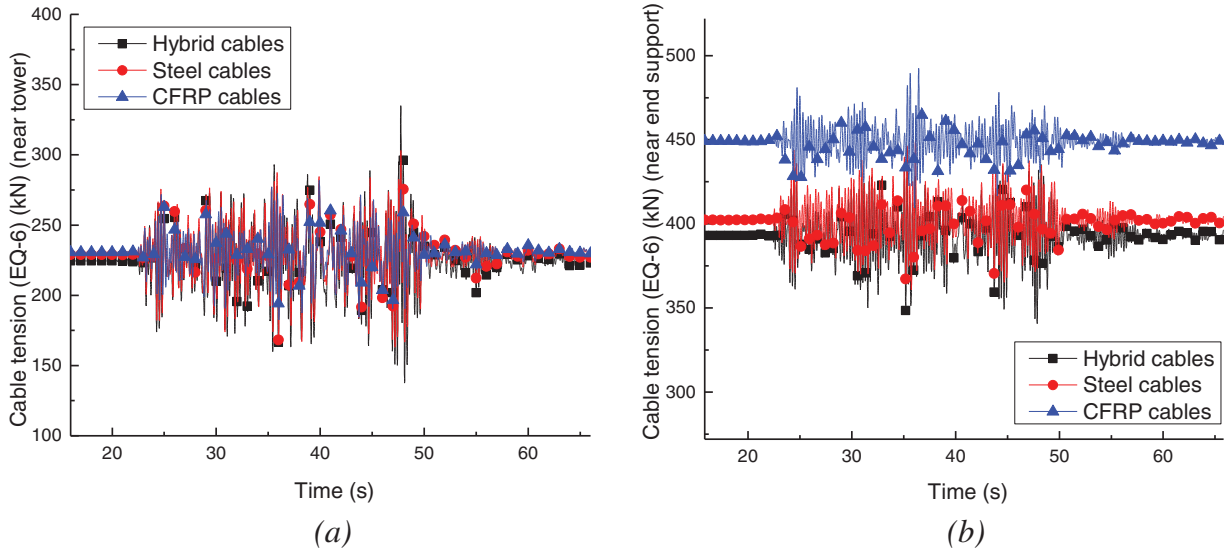

Figure 17. Time–history plot for cable forced for (a) shortest cable and (b) longest cable. CFRP, carbon fiber–reinforced polymer

Table 7. Statistics and percentile for different response quantities of interests

Response quantities	HSCs					SSCs				
	Range (max–min)	Mean (μ)	Standard deviation (σ)	50th	90th	Range (max–min)	Mean (μ)	Standard deviation (σ)	50th	90th
Deck vertical displacement (mm)	60–07	23	0.0139	19	41	60–7	24.1	0.015	19	43
Tower displacement-X (mm)	30.4–3.8	15.03	0.008	11.66	28.391	32–3	15	0.008	11	28
Tower displacement-Y (mm)	212.8–21.78	97.57	0.05	92.6	175.77	213–21	97	0.05	94	175
Cable force near tower-99 (kN)	335.9–235.6	268.9	25.454	259.45	301.22	237.84–315.7	267.88	21.685	262.23	299.67
Cable force near end-114 (kN)	448.9–399.5	419.08	15.059	413.34	444.02	451.9–407	424.77	13.34	421.22	443.62
Deck moment (MN.m) M_y	0.98–0.10	0.47	0.247	436.25	806.84	1.18–0.24	0.56	0.25	0.4991	0.8421
Overturning moment (MN.m) M_y	105.4–10.52	35.3	20.145	33.3	56.8	112.83–9.88	37.06	21.97	33.59	60.242
Torsional moment (MN.m) M_z	144.4–12.1	51.9	37.6	32.6	109.2	145.21–12.48	51.23	37.731	32.647	109.44

Note: HSC, hybrid stay cable; SSC, steel stay cable

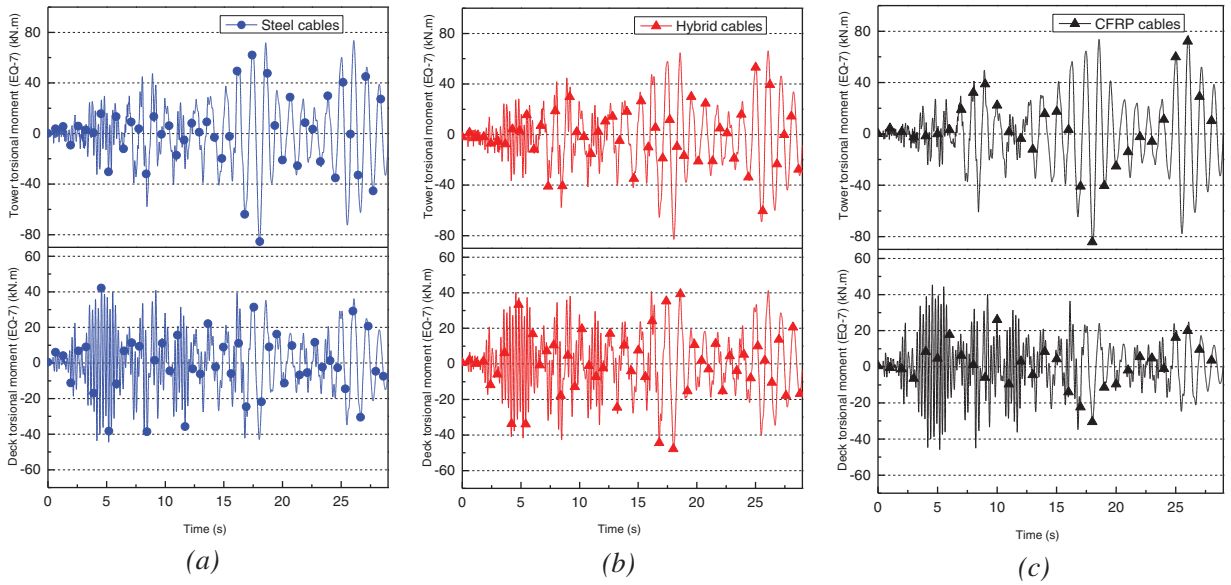

Figure 18. Time–history plot of the torsional moment in tower and deck for (a) steel stay cables (SSCs) and (b) hybrid stay cables (HSCs), and (c) carbon fiber–reinforced polymer (CFRP) stay cables

Table 7 shows the maximum and minimum range, mean, standard deviation, and 50th and 90th percentiles for the response QoIs. The mass reduction from CFRP (~40% lighter than steel) and its interaction with the steel shell also modify the global dynamic properties of the bridge. The hybrid cables increased the fundamental frequency (by ~3%) and shifted energy input across vibration modes. Additionally, the bonded steel–CFRP interface contributes to enhanced damping through frictional effects. Under extreme seismic conditions, the staged failure mode, where CFRP fractures first and steel yields progressively, offers resilience against catastrophic failure. These attributes make hybrid cables particularly promising for bridges in seismically active zones.

Fig. 18 shows the time history of torsional moments in both the tower and the deck for the three stay cable configurations. Each cable material exhibits a distinct influence on the torsional behavior under seismic loading. For steel cables (SSC), the maximum torsional moment in the tower occurs early during excitation, indicating a quicker response to seismic input. In contrast, hybrid cables (HSC) show a delayed peak with a significant phase difference, suggesting altered dynamic interaction due to their lower mass and different axial stiffness.

The case of CFRP cables, with the highest stiffness-to-weight ratio, also exhibits a distinct torsional response. The moment pattern exhibits higher fluctuation density and delayed peaks relative to SSC, indicating sensitivity to higher

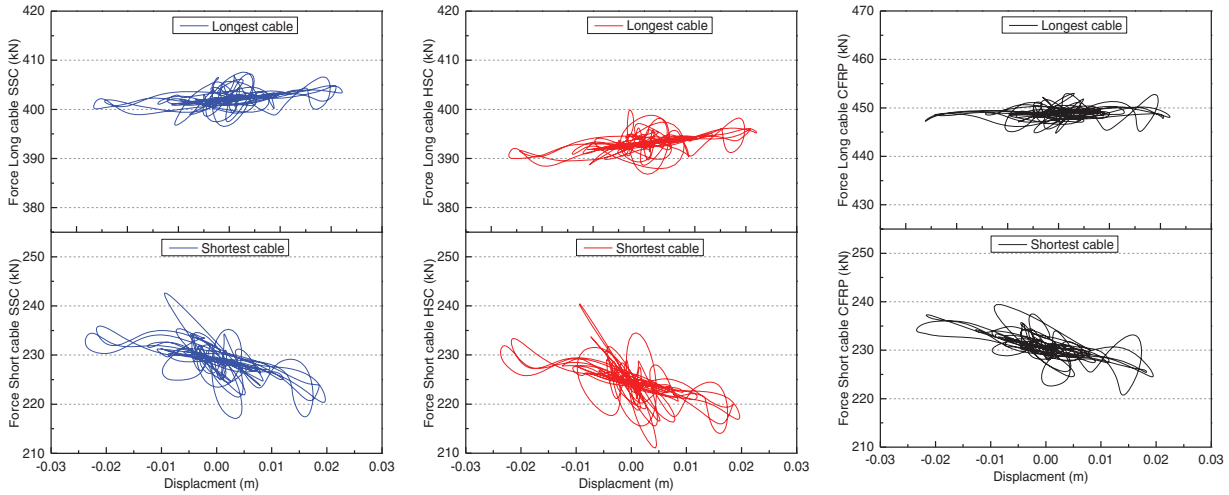

Figure 19. Tension–displacement cyclic responses of the longest and shortest stay cables under seismic excitation. CFRP, carbon fiber–reinforced polymer; HSC, hybrid stay cable; SSC, steel stay cable

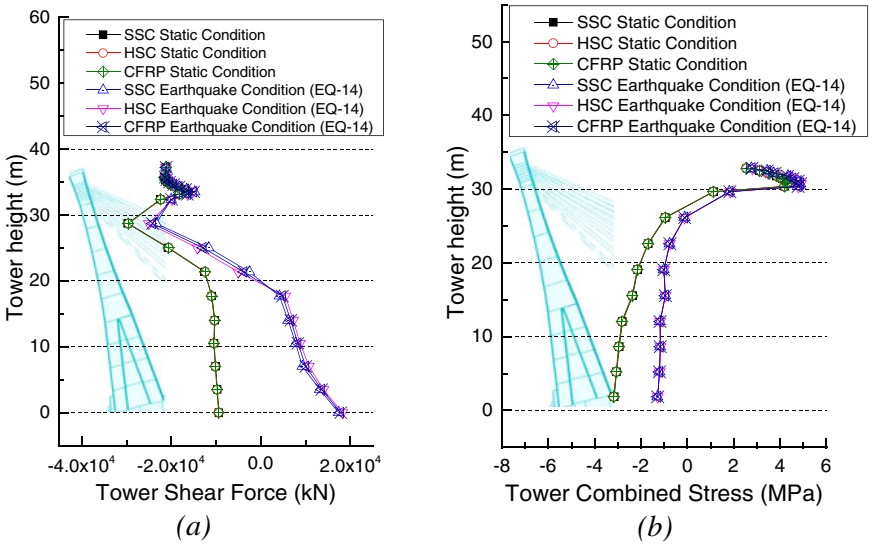

Figure 20. Maximum peak response along the height of the tower for (a) shear force and (b) combined stress. CFRP, carbon fiber–reinforced polymer; HSC, hybrid stay cable; SSC, steel stay cable

vibration modes. These variations indicate that the cable material plays a crucial role in governing torsional dynamics, especially in multidirectionally excited systems.

To better highlight these differences, Fig. 19 shows the tension–displacement plots of the longest and shortest stay cables under seismic excitation, providing further insight into the three cable systems. In the SSC configuration, the loops exhibit wider, more irregular shapes, particularly in the shorter cables. In contrast, the HSC system exhibits comparatively narrower, more stable loops, reflecting an improved retention of axial stiffness under dynamic loading. The CFRP cables exhibit the most linear force–displacement relationship, confirming their high stiffness-to-mass ratio and reduced internal damping contribution.

These differences are directly related to the axial stiffness and mass characteristics of the cable materials. Steel cables, with higher mass and lower specific stiffness, allow larger displacement amplitudes, thereby increasing the exchange of cyclic strain energy and localized damping. Hybrid cables, combining reduced mass with enhanced stiffness, moderate this behavior by limiting excessive deformation while still participating in dynamic energy redistribution. Pure CFRP systems, due to their lower density and higher modulus, shift the dynamic response toward a more regular regime and enhance global stiffness.

Overall, while the global seismic response of the bridge remains deck-dominated, the cable material properties influence the redistribution of kinetic and strain energy within the structure. The HSC configuration demonstrates a balanced response, reducing excessive deformation observed in SSC while avoiding the overly stiff response of pure CFRP cables.

Fig. 20 presents the variation of tower shear force and combined stress under both static and earthquake loading conditions for all three cable types (SSC, HSC, and CFRP). In terms of shear force (Fig. 19a), an uneven distribution is

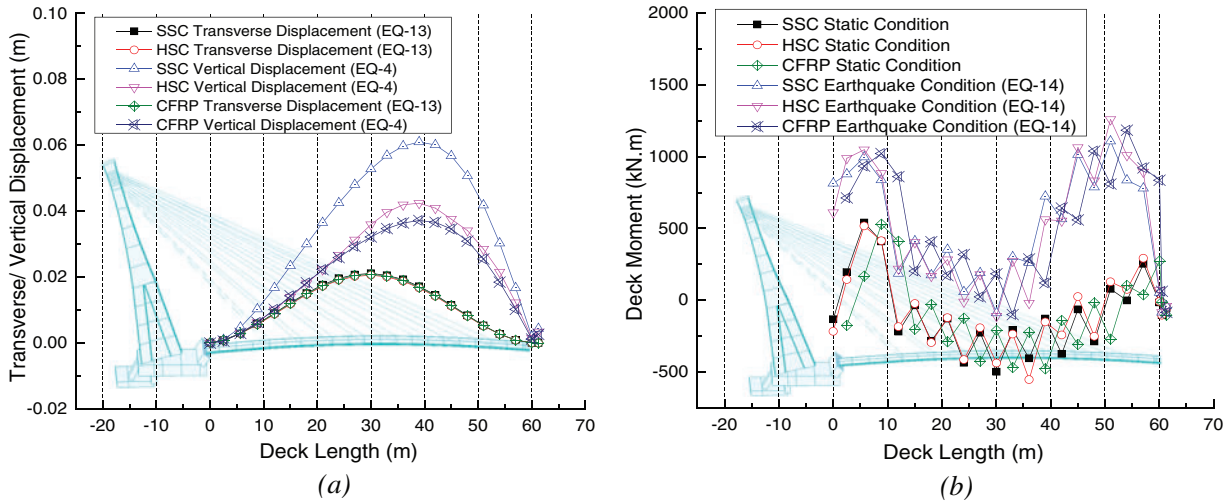

Figure 21. Maximum response of the bridge deck for SSC and HSC. (a) Transverse/vertical displacement and (b) deck moment profile. CFRP, carbon fiber–reinforced polymer; HSC, hybrid stay cable; SSC, steel stay cable

visible near the top of the tower, likely caused by the concentrated pull force from the connected stay cables. Among the three, the CFRP configuration exhibits a slightly lower peak shear force under earthquake conditions compared to SSC and HSC. This difference is primarily due to CFRP's higher initial static tension and lower self-weight, which alter the force transfer to the tower. These findings align with trends reported in previous studies using fiber-based cables.[26,27]

As shown in Fig. 20b, the combined stress in the tower peaks near the top region for all configurations. Again, the CFRP system presents a similar overall stress distribution to SSC and HSC, but with slightly reduced magnitude, indicating a moderate benefit in tower stress control under seismic actions. The overall variations between the three systems remain minor in terms of stress, suggesting that the global load path remains consistent regardless of the cable type used.

Fig. 21a presents the deck displacement profiles under earthquake loading in both vertical and transverse directions. The maximum vertical displacement occurs at mid-span for all cable types. However, transverse displacement is observed in all three configurations. SSC, with the highest axial stiffness, shows greater transverse movement than HSC and CFRP systems. CFRP cables exhibit the lowest transverse displacements, likely due to their favorable stiffness-to-weight ratio, which reduces inertial effects. The maximum transverse displacement across all earthquake records is noted for EQ-13 near the free end, with SSC reaching approximately 20 mm.

Fig. 21b shows the distribution of the deck moment (My) under both static and seismic conditions. Under seismic loading, CFRP cables result in noticeably reduced peak bending moments compared to SSC and HSC, indicating improved dynamic efficiency. Under static conditions, the moment diagram shows a positive peak near the tower and a negative peak near mid-span. This is consistent with the asymmetrical geometry and support configuration of the bridge, where the positive moment represents tension in the bottom fibers near the pylon, while the negative mid-span moment reflects tension in the top fibers. Overall, the CFRP system leads to a balanced reduction in both vertical displacement and seismic moment intensity. The moment distribution is similar for both HSC and SSC cases under static and earthquake loading conditions. Also, a similar change can be seen in existing literature with fiber stay cables.[26,27]

Fig. 22 shows cable force distribution for two different ground motions along the geometric profile of the bridge under static and earthquake loading for both SSC and HSC cases. The maximum peak response is located near the tower and at the end support away from the tower. For the behavior of the cables under earthquake loading, HSC shows a higher percentage change than SSC. This rate of change is quite noticeable for the cables with element numbers from 105 to 110, which, in effect, causes the higher deck moment, as seen in Fig. 21b.

Corrosion effects on SSCs

During the long service life of stay cables, corrosion is a major concern. This section assesses how conventional SSCs degrade over time due to uniform corrosion and compares their performance with that of corrosion-resistant options, such as hybrid cables.[9,29] The hybrid strands studied comprise super-austenitic stainless steel, which is effective in protecting against chloride-rich environments. Additionally, galvanic corrosion is prevented by electrically isolating the shell from the CFRP core. Although residual stresses can lead to stress–corrosion cracking, these issues are manageable with proper welding and posttreatment.

The analysis is inspired by the methodology presented in Vikas et al.,[30] applying Lemaitre's equivalent strain principle to quantify loss of stiffness and strength. The corrosion effect was modeled as a uniform reduction in cross-sectional

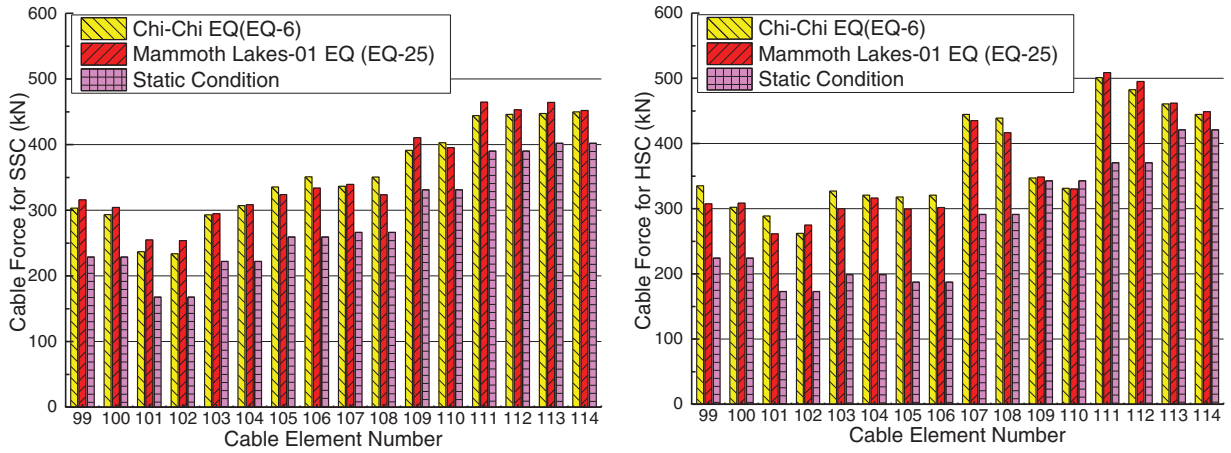

Figure 22. Maximum peak values of stay cable forces under static and earthquake loading for SSC and HSC. HSC, hybrid stay cable; SSC, steel stay cable

Table 8. Modified values of modulus of elasticity and UTF for different corrosion levels for SSC

Corrosion (%)	Diameter (mm)	E_eff (GPa)	UTF (kN)	Frequency (Hz)
0	*37*	*165.00*	*1761.4*	*0.952*
5	*36.06*	*156.75*	*1673.1*	*0.952*
10	*35.1*	*148.50*	*1584.9*	*0.952*
15	*34.11*	*140.25*	*1496.6*	*0.942*
20	*33.09*	*132.00*	*1408.3*	*0.914*
25	*32.04*	*123.75*	*1320.0*	*0.886*
30	*30.96*	*115.50*	*1231.7*	*0.855*
33.5	*30.17*	*109.13*	*1171.1*	*0.832*
35	*29.83*	*106.88*	*1145.1*	*0.820*
40	*28.66*	*98.63*	*1056.8*	*0.791*

Note: UTF, ultimate tensile force.

area of the cable. According to Lemaitre (1971), the effective Young's modulus of a corroded cable $\tilde{E}$ is calculated as

$$\tilde{E} = E \cdot \frac{A^*}{A_0} \tag{4}$$

where E is the original Young's modulus, A_0 is the original cross-sectional area, and A^* is the reduced area due to corrosion. Furthermore, the ultimate tensile force (UTF) of the corroded cable is derived by multiplying the remaining area with the original ultimate tensile strength of steel:

$$\text{UTF} = \sigma_u \cdot A^* \tag{5}$$

where σ_u is the ultimate strength of steel (1640 MPa).

The following table shows the progressive degradation in the elastic modulus and UTF with increasing corrosion percentage, starting from the original cable diameter of 37 mm (area = 1.074 cm^2).

At 33.5% area loss, the cable reaches its ultimate tensile capacity, beyond which failure is expected. The elastic modulus reduces linearly with corrosion, resulting in significant flexibility in the structural response. As shown in Table 8, the frequencies decrease progressively with increasing corrosion levels. While the reduction is modest up to 15% corrosion, a more noticeable decline begins beyond 20%, indicating a gradual loss of stiffness and mass distribution efficiency. This trend highlights the sensitivity of dynamic response to material degradation and suggests that frequency monitoring could serve as a useful indicator for assessing the health and structural integrity of stay cables under corrosive environments.

It can be seen from Fig. 23 that the displacement contours illustrate the progressive loss of stiffness in corroded SSCs. For the SSC system, the maximum deck displacement increases from 0.31 m at 30% corrosion to 0.35 m at 33% corrosion and reaches 0.46 m at 40% corrosion, indicating a rapid deterioration in global structural performance as the cable cross-section and elastic modulus reduce. In contrast, the HSC system exhibits a significantly lower displacement of 0.24 m under the same loading conditions. This improvement is attributed to the corrosion-resistant CFRP core and stainless-steel shell, which preserve axial stiffness and tensile capacity even as external degradation accumulates. Overall, the results indicate that hybrid cables exhibit a more stable displacement response and maintain structural integrity better than conventional steel cables under severe corrosion conditions.

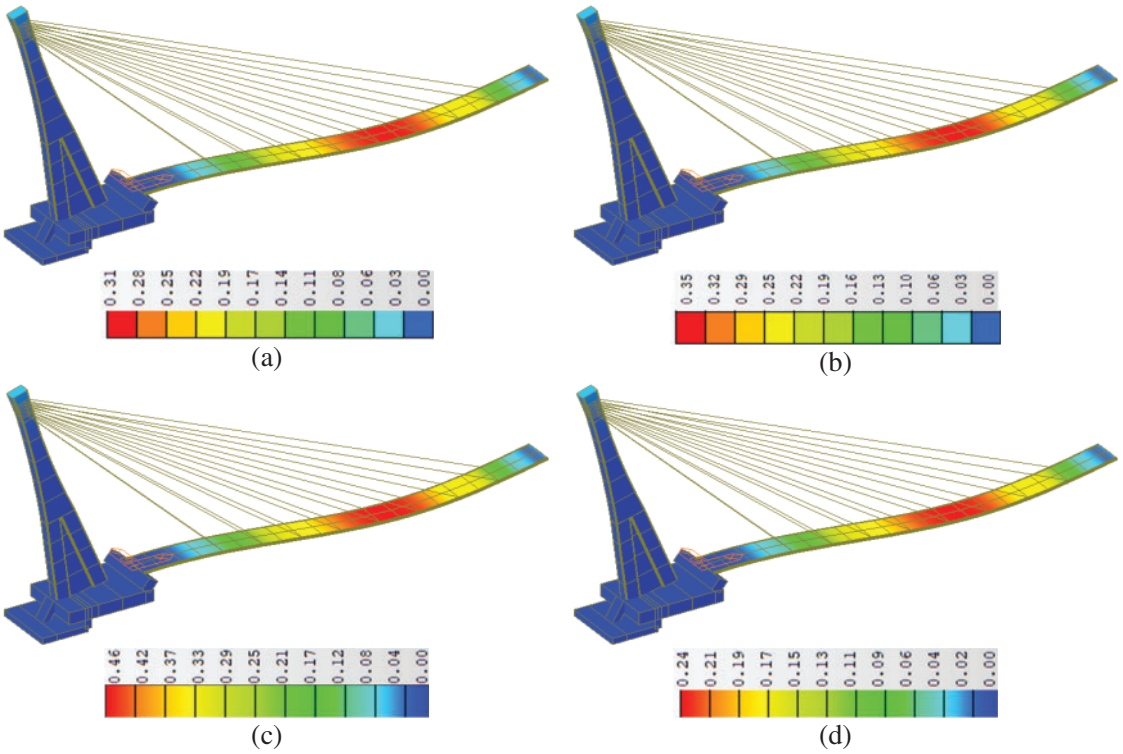

Figure 23. Displacement (in m) contours of the bridge under different steel-cable corrosion levels and comparison with the HSC corrosion-resistant solution: (a) displacement contour with SSC at 30% corrosion, (b) displacement contour with SSC at 33% corrosion, (c) displacement contour with SSC at 40% corrosion, and (d) displacement contour with HSC. HSC, hybrid stay cable; SSC, steel stay cable

Corrosion can lead to significant degradation of both mechanical performance and structural safety over time. As observed in the results, such degradation can lead to noticeable increases in bridge deck deflection, on the order of 6%–7% near the end supports, even before complete failure. The loss of stiffness due to corrosion has further implications beyond localized deformation. As the modulus of elasticity decreases, the affected cables exhibit lower resistance to axial loads, thereby altering the structure's natural frequencies and amplifying dynamic responses under transient loads such as pedestrian movement or wind. Over time, this can lead to vibration discomfort for users or even resonance phenomena in more severe cases.

As shown in Fig. 24, the moment contours indicate that the maximum bending moment in the bridge deck increases significantly from 38775.66 kNm in the uncorroded (0%) state to 48377.78 kNm under 40% corrosion. This nearly 25% increase reflects the loss of effective cable stiffness and axial capacity due to section degradation, thereby shifting more bending demand to the deck and tower. In contrast, HSCs offer better, albeit limited, corrosion resistance, thereby maintaining a more uniform force distribution and minimizing additional moment demands on the structure.

More critically, cable corrosion introduces the risk of force redistribution and progressive failure. When a severely corroded cable fails, the load it was carrying must be instantly transferred to adjacent cables. If the failed cable is located near the tower, this redistribution concentrates load in the shortest, most stressed cables, increasing the likelihood of overload and sequential failures. Similarly, failure of a cable near midspan, although it spreads the redistribution over more cables, still risks local overstressing and structural instability. Without sufficient redundancy or reserve capacity in the system, this cascading effect can compromise the integrity of the entire bridge. Remedial strategies typically involve frequent inspection cycles, nondestructive testing of internal corrosion, application of protective coatings, or the use of internal filling materials such as wax or resin. In many cases, full cable replacement becomes necessary every 25–35 years, significantly adding to the bridge's maintenance burden and life-cycle cost.

In contrast, hybrid cables and CFRP tendons exhibit better long-term performance in corrosive environments. Their material composition shields them from aggressive chemical attack, and their mechanical properties remain stable even under severe environmental exposure. While these advanced materials entail higher initial costs, they eliminate the need for frequent maintenance, prevent progressive collapse, and extend the bridge's service life. It should be noted that the present corrosion analysis assumes uniform cross-sectional reduction along the cable length. In reality, corrosion mechanisms may be localized, pitting-based, or influenced by anchorage conditions and moisture accumulation, leading to nonuniform stiffness degradation and stress concentration effects. While the uniform reduction approach provides a conservative and analytically tractable

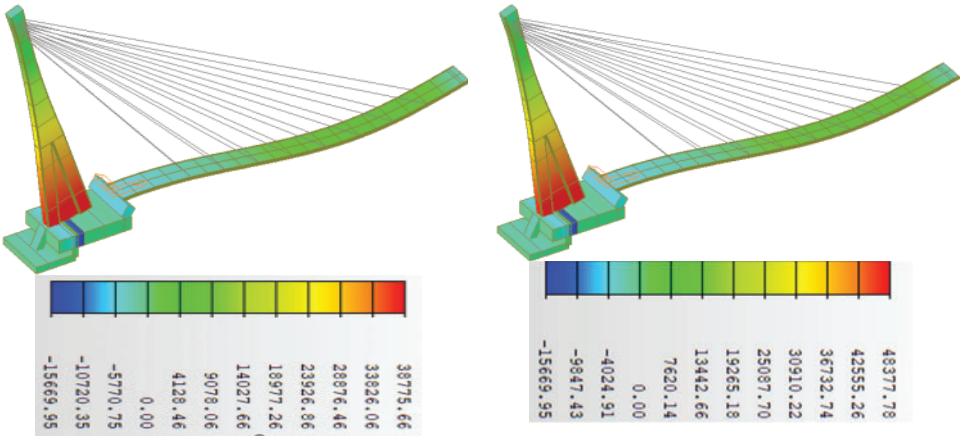

(a) *(b)*

Figure 24. Moment (kN.m) contour with SSC at (a) 0% and (b) 40% corrosion of stay cables. SSC, steel stay cable

representation of long-term degradation, future studies may incorporate localized corrosion modeling or probabilistic deterioration scenarios to capture more realistic damage patterns.

Conclusions

This study assessed the applicability of hybrid steel-CFRP stay cables in cable-stayed bridges through experimental characterization and structural analysis. By comparing full steel (SSC), hybrid (HSC), and full CFRP cable configurations under both static and seismic conditions, and incorporating long-term degradation from corrosion, the research provides a more comprehensive understanding of cable system selection in modern bridges.

- Experimental testing confirmed the hybrid wire's structural capacity, with high stiffness up to steel yielding and tensile strengths exceeding 1400 MPa, despite geometric and twisting effects. The hybrid assembly offers a favorable balance between mechanical strength and weight efficiency.
- The HSC configuration maintains relatively uniform tension across different lengths due to the compensating effect of CFRP's higher stiffness. In contrast, steel cables display pronounced fluctuations in cable force distribution. This behavior improves load-sharing and facilitates optimized cable layout strategies.
- Bridges with CFRP and hybrid cables showed slightly higher natural frequencies than the steel-only version, owing to lower mass and altered dynamic stiffness. Although these frequency shifts are modest and mode shapes remain comparable, the results emphasize the influence of stay cable materials on dynamic response.
- Seismic results reveal minimal differences in overall stress and moment contours between SSC and HSC systems, while CFRP cables exhibit higher axial forces due to their initial tension and higher modulus. Displacement and deck moment variations are more pronounced in the CFRP solution, especially in longer cables. Hybrid systems, however, provide a better compromise by mitigating dynamic amplification while maintaining structural compatibility.
- Under increasing corrosion scenarios, SSC-based systems show a notable drop in performance, with bending moment increasing by over 25% and deck displacement rising significantly. In contrast, the HSC configuration remains stable due to its corrosion-resistant CFRP core. This highlights the critical advantage of hybrid cables in long-term durability and structural safety.

From a practical standpoint, the results suggest that hybrid cable systems offer a balanced compromise between mechanical performance and long-term durability, particularly for retrofit or corrosion-prone environments. However, the present study is limited to numerical simulations of a representative pedestrian cable-stayed bridge and does not include full nonlinear seismic time-history interaction with cable damage evolution. Further research should address life-cycle assessment, anchorage behavior, and probabilistic corrosion modeling to support implementation in large-scale bridge design.

Acknowledgments

This work was carried out with a financial grant from the Research Fund for Coal and Steel of the European Union, within the EU project FIRST-WIRE "FIber Reinforced STeel WIREs for high-performance, lightweight ropes and cables operating in demanding scenarios" (Grant RFCS-2019-899299). This study was also supported by FABRE—"Research Consortium for the Evaluation and Monitoring of Bridges, viaducts and other structures" (www.consorziofabre.it/en).

References

[1] Wang R, Xu Y, Li J. Transverse seismic behavior studies of a medium span cable-stayed bridge model with two concrete towers. *J Earthquake Eng*. 2017;21(1):151–168. Taylor and Francis Ltd. doi:10.1080/13632469.2015.1118710.

[2] Galvín P, Domínguez J. Dynamic analysis of a cable-stayed deck steel arch bridge. *J Construct Steel Res*. 2007;63(8):1024–1035. Elsevier. doi:10.1016/j.jcsr.2006.11.001.

[3] Xiong W, Cai CS, Zhang Y, Xiao R. Study of super long span cable-stayed bridges with CFRP components. *Eng Struct*. 2011;33(2):330–343. doi:10.1016/j.engstruct.2010.10.013.

[4] Savor Z, Radic J, Hrelja G. Cable vibrations at Dubrovnik bridge. *Bridge Struct*. 2006;2(2):97–106. doi:10.1080/15732480600855800.

[5] Tuladhar R, Dilger WH, Elbadry MM. Influence of cable vibration on seismic response of cable-stayed bridges. *Canadian J Civil Eng*. 1995;22(5):1001–1020. doi:10.1139/l95-116.

[6] Almansour HH. The performance of hybrid long-span cable stayed bridges using advanced composites; 2006.

[7] Li H, Ou J. The state of the art in structural health monitoring of cable-stayed bridges. *J Civil Struct Health Monitor*. 2016;6:43–67. Springer Berlin Heidelberg.

[8] Liang Y, Zhao T, Wei Y, Guan P. Fragility analysis of cross-sea highway cable-stayed bridges under seismic-wind combined loading. *Eng Fail Anal*. 2025;173(January):109451. Elsevier Ltd. doi:10.1016/j.engfailanal.2025.109451.

[9] Sun H, Xu J, Chen W, Yang J. Time-dependent effect of corrosion on the mechanical characteristics of stay cable. *J Bridge Eng*. 2018;23(5):1–13. doi:10.1061/(asce)be.1943-5592.0001229.

[10] Yi J. Modeling and analysis of cable vibrations in cable-stayed bridges under near-fault ground motions. *Eng Struct*. 2023;277(August 2022):115443. Elsevier Ltd. doi:10.1016/j.engstruct.2022.115443.

[11] Ai P, Ding G, Li Z, Feng P. Long-term creep behavior of novel self-anchored CFRP cable system. *Compos Struct*. 2024;334(2):117965. Elsevier. doi:10.1016/j.compstruct.2024.117965.

[12] Liu Y, Zwingmann B, Schlaich M. Carbon fiber-reinforced polymer for cable structures-A review. *Polymers*. 2015;7(10):2078–2099. MDPI AG. doi:10.3390/polym7101501.

[13] Long G, Sun Y, Shang Z, Wang X, Xu X, Wang T. Aerodynamic performance and wind-induced response of carbon fiber-reinforced polymer (CFRP) cables. *Scient Rep 2024 14:1*. 2024;14(1):1–20. Nature Publishing Group. doi:10.1038/s41598-024-59002-w.

[14] Sun Y, Mei K, Sun S, Wang T, Ren X. Optimal design of a novel composite anchorage for carbon-fiber-reinforced polymer (CFRP) tendons. *Polymers*. 2022;14(10):2048. MDPI. doi:10.3390/polym14102048.

[15] Cai H, Aref AJ. On the design and optimization of hybrid carbon fiber reinforced polymer-steel cable system for cable-stayed bridges. *Compos Part B: Eng*. 2015;68:146–152. Elsevier Ltd. doi:10.1016/j.compositesb.2014.08.031.

[16] Wang X, Wu Z. Integrated high-performance thousand-metre scale cable-stayed bridge with hybrid FRP cables. *Compos Part B: Eng*. 2010;41(2):166–175. doi:10.1016/j.compositesb.2009.09.001.

[17] Yang Y, Wang X, Wu Z. Long-span cable-stayed bridge with hybrid arrangement of FRP cables. *Compos Struct*. 2020;237. Elsevier Ltd.

[18] Karbhari VM. *Use of composite materials in civil infrastructure in Japan. International Technology Research Institute*. International Technology Research Institute World Technology (WTEC) Division; 1998.

[19] Meier H, Brönnimann U. Zwei CFK-Kabel für die Storchenbrücke Zwei CFK-Kabel für die Storchenbrücke. *SCHWEIZER INGENIEUR UND ARCHITEKT-SCHWEIZERISCHE BAUZEITUNG*. 1996;114.

[20] Dassault Systèmes Simulia. ABAQUS 6.12-example problems manual volume 1. *Abaqus 6.12*. 2012a;II:14.1–14.14.

[21] Nascimbene R. An arbitrary cross section, locking free shear-flexible curved beam finite element. *Int J Computat Meth Eng Sci Mech*. 2013;14(2):90–103. doi:10.1080/15502287.2012.698706.

[22] Dassault Systèmes. *Abaqus Benchmarks Manual (Version 6.12)*. Vélizy-Villacoublay, France: Dassault Systèmes Simulia Corp; 2012.

[23] Hassan MM, Nassef AO, El Damatty AA. Determination of optimum post-tensioning cable forces of cable-stayed bridges. *Eng Struct*. 2012;44(2):248–259. Elsevier Ltd. doi:10.1016/j.engstruct.2012.06.009.

[24] Midas IT. Analysis for civil structures; 2012. p. 389

[25] Yu B, Gao S, Gao C, Yang J, Xie B. The determination of the problem of the cable-stayed bridge reasonable superpositioning optimization under the constant load state, basing on the unknown load coefficient method of midas/civil. *Appl Mech Mat*. 2012;178–181:2081–2084. doi:10.4028/www.scientific.net/amm.178-181.2081.

[26] Xie G-H, Yin J, Liu R-G, Chen B, Cai D-S. Experimental and numerical investigation on the static and dynamic behaviors of cable-stayed bridges with CFRP cables. *Compos Part B: Eng*. 2017;111(2):235–242. Elsevier Ltd. doi:10.1016/j.compositesb.2016.11.048.

[27] Ren L, Fang Z, Wang K. Design and behavior of super-long span cable-stayed bridge with CFRP cables and UHPC members. *Compos Part B: Eng*. 2019;164(August 2018):72–81. Elsevier. doi:10.1016/j.compositesb.2018.11.060.

[28] Giannini R, Paolacci F, Phan HN, Corritore D, Quinci G. A novel framework for seismic risk assessment of structures. *Earthquake Eng Struct Dynam*. 2022;51(14):3416–3433. doi:10.1002/eqe.3729.

[29] Pang Y, Wei K, He H, Wang W. Assessment of lifetime seismic resilience of a long-span cable-stayed bridge exposed to structural corrosion. *Soil Dynam Earthquake Eng*. 2022;157(March):107275. Elsevier Ltd. doi:10.1016/j.soildyn.2022.107275.

[30] Vikas AC, Prashanth MH, Gogoi I, Channappa TM. Effect of cable degradation on dynamic behavior of cable stayed bridges. 2013;3(1):35–45.